UPTEC F07 033
Examensarbete 20 p
Mars 2007

Low Frequency Radio Astronomy & Extrasolar Planet Detection

Jonatan Danielsson

UPPSALA
UNIVERSITET

Teknisk- naturvetenskaplig fakultet
UTH-enheten

Besöksadress:
Ångströmlaboratoriet
Lägerhyddsvägen 1
Hus 4, Plan 0

Postadress:
Box 536
751 21 Uppsala

Telefon:
018 – 471 30 03

Telefax:
018 – 471 30 00

Hemsida:
http://www.teknat.uu.se/student

Abstract

Low Frequency Radio Astronomy & Extrasolar Planet Detection

Jonatan Danielsson

In our solar system all planets with a magnetic field produce and emit radio waves. It originates from the interaction between the solar wind and the planetary magnetic field. In this diploma thesis the possibility to detect radio emissions from extrasolar planets has been investigated, including basic concepts of low frequency radio astronomy and some concepts of future observatories in space able to detect emissions below the ionospheric cut-off frequency around 10 MHz, which is required for detection of planets smaller then the size of Jupiter. From all extrasolar planets, already detected with other methods, their flux densities in the radio frequency band were calculated and seven candidates were found that should be detectable with an antenna array with the size of the full LOFAR, which is under construction in the Netherlands. To be able to detect planets smaller then Jupiter, a large space based array is needed. The Moon is a suitable location for such an array, where a dense array on the surface can be combined with antennas in different orbits to achieve sufficient sensitivities and spatial resolutions.

Handledare: Jan Bergman
Ämnesgranskare: Jan Bergman
Examinator: Tomas Nyberg
ISSN: 1401-5757, UPTEC F07 033

Contents

Chapter 1

Introduction

1.1 History of Radio Astronomy

The development in low frequency radio astronomy has come to the border where single dish antennas with sufficient angular resolution and sensitivity have become impossible to construct. Since the resolution is directly proportional to the collecting area of the telescope, the only way to achieve higher spatial resolution is to build larger telescopes. For observations in the MHz frequency range, collecting areas of hundreds of square kilometers are needed, which of course is impossible to achieve with a single dish antenna. For example the 305 m diameter Arecibo radio telescope, the worlds largest single dish, observing at 100 MHz, have an angular resolution of approximately 30 arcminutes. In the optical range, on the other hand, a 8 meter telescope will have a diffraction limit as small as 0.01 arcsecond, *i.e.* about 200 000 times better with a 1000 times smaller aperture area.

For low frequency radio astronomy, instead of building single dish antennas it is convenient to use short dipole antennas, because their effective area is proportional to the wavelength squared. So, when the frequency decreases the wavelength increases, and hence the aperture size increases. Then, by combining several short dipoles into an array of antennas spread over a large area, it is possible to synthesize a dish antenna, this is called *aperture synthesis*. And then, by using interferometry, the outputs from each antenna is combined with all the other antennas, forming the desired measurement or image.

In the beginning of the 1930s, Karl Jansky was investigating the source of static that could interfere with transatlantic telephone transmissions. He built an antenna designed to receive signals at 20.5 MHz and recorded them from all directions during several months. He categorized the static into three different groups: nearby thunderstorms, distant thunderstorms, and a faint steady hiss of unknown origin [10]. After spending several months in investigating the third type of static, he eventually figured out that it originated from the Milky Way, with the strongest emission coming from the center. The discovery was published in New York Times, on May 5, 1933, and can be referred to as the first modern detection of an extraterrestrial radio source.

In 1946, Martin Ryle, and his group in Cambridge, introduced the the concept of radio interferometry. The signals from two antennas were added electron-

Figure 1.1: The Very Large Array (VLA): View of the telescope close together.

ically to produce interference. For this and future work in aperture synthesis, Sir Martin Ryle and Antony Hewish were awarded with the Noble Prize in physics 1974. Hewish for his decisive role in the discovery of pulsars.

One of the most important discoveries in radio astronomy was the detection of the 21 cm spectral hydrogen line in 1951. The hydrogen line had earlier been predicted in 1944 by Oort and van de Hulst [5]. The importance of a spectral line lies in the possibility to observe the Doppler shift of the line frequency; thus measuring the radial velocity of objects, which would provide the astronomers with a powerful tool.

Since those first discoveries of extraterrestrial radio emissions, the development of high resolution radio telescopes has been an ongoing process. The simple two-element interferometers with high angular resolution were improved to be able of making full images, using aperture synthesis techniques, and the development of *Very Large Baseline Interferometry* (VLBI) in the 1960s resulted in a large improvement of angular resolution. One of the most successive telescopes constructed is the Very Large Array (VLA), which was built in the 1970s in New Mexico. It consists of 27 large 25 m diameter full steerable dish antennas in a Y-shape configuration, see Fig. 1.1, observing in frequencies from 74 MHz up to 50 GHz. For a more complete review of the development of high resolution radio astronomy see Kellerman and Moran, 2001 [11].

VLA and similar large interferometric arrays have their restrictions in the data/signal processing. As the number of antennas increases, the computational power to process all signals basically increases with the number of antennas squared, thus setting a limit depending on available computer processing power.

Today's supercomputers have moved the development in a new direction, instead of building arrays of a few large dish antennas, the new radio telescopes consist of several thousands of short dipoles located over large areas. All signals received are then stored digitally and correlated in software by state of the art supercomputers. One example is the LOw Frequency ARray (LOFAR)

Figure 1.2: The LOw Frequency ARray (LOFAR): Antenna station array configuration.

under construction in the Netherlands, see Fig. 1.2, which uses a 10 000 CPU supercomputer (IBM Blue Gene/L) to perform the signal processing.

1.2 The radio frequency band

This diploma thesis concentrate on observations in the radio frequency (RF) band. The RF band stretches over a wide frequency range from very low frequencies (a few Hz) to very high frequencies (100 GHz). A single telescope can not cover the whole span. For very low frequencies it is convenient to use dipole antennas because of the long wavelength. As the wavelength becomes shorter the effective area of dipoles decreases and it becomes more useful to construct dish antennas. Because the topic for this thesis is to investigate the use of low frequency arrays all antennas will be regarded as dipole antennas. However, the theory is general and works for all types of antennas.

The purpose of a radio telescope is to detect radiation from cosmic sources. The radiation is referred to as *signals* and induces a voltage in the antennas. Cosmic signals are generated by natural processes and usually have the form of Gaussian random noise. They are also invariant within timescales of minutes or hours, which is typically the duration of a radio observation. The radiation can also be regarded as continuum radiation. Hence, the power spectrum is constant over the receiving bandwidth. Waveforms with those properties can be assumed to be stationary and ergodic [4].

Chapter 2

Two-element interferometer

2.1 Background

This chapter will cover the fundamentals in radio astronomy with interferometric arrays, starting with some explanations of commonly used concepts. Then the response of a two-element interferometer is derived, followed by geometrical relationships between the source and the observer, and finally the basic formulas for the performance of an array are derived.

2.2 Basic Concepts in Radio Astronomy

2.2.1 Aperture Synthesis

Each pair of antennas in an array, samples a spatial Fourier component of the radio source brightness distribution at a given instant in time. Moving the antennas to different locations, and again measuring the Fourier components, will synthesize an aperture. If all possible locations in space are covered the array will synthesize an aperture comparable to a single dish antenna with diameter equal to the array's maximum baseline.

One way to synthesize a larger aperture is to use the rotation of Earth around its own axis. As illustrated in Fig. 2.1, rotation of Earth effectively synthesize a single aperture in 12 hours. This is called *Earth Rotation Aperture Synthesis*.

It is also possible to synthesize a larger aperture with only two antennas. If one is moveable, for example mounted on a rail track, the antennas can measure the Fourier components during one 12 hour observation to get a complete elliptical locus in the plane. Then by moving one antenna, and do a new 12 hour observation, another locus is obtained. Repeating this procedure will eventually fill the whole plane.

2.2.2 Jansky

In radio astronomy, a suitably unit expressing the strength of a received radio signal from a discrete source is Jansky [Jy], named after the pioneering radio astronomer Karl Jansky.

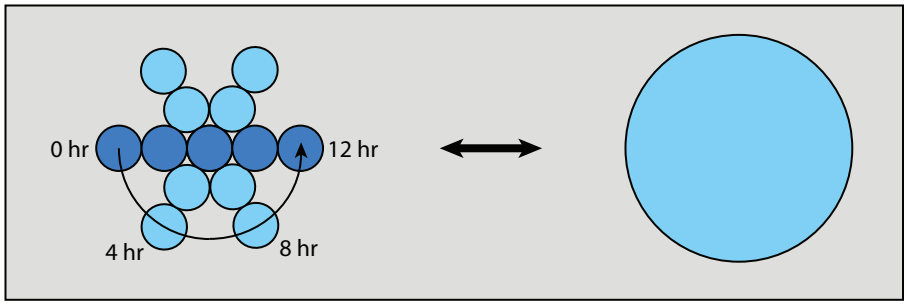

Figure 2.1: The principle behind Earth rotation aperture synthesis. Imagine an observer located above the north pole looking down at the array. As the Earth rotate the line, in which the antennas are located, will sweep portions of a filled aperture, and in 12 hours it will synthesize a complete circular aperture.

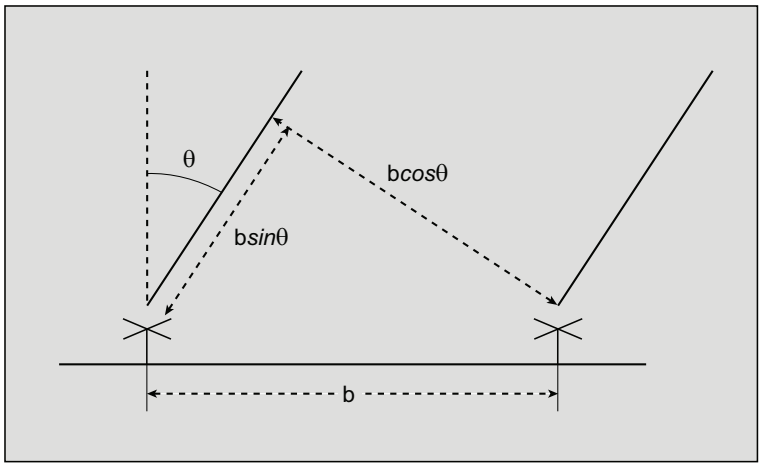

Figure 2.2: The setup of a basic two-element interferometer

In SI units, $1\text{Jy} = 10^{-26}\text{Wm}^{-2}\text{Hz}^{-1}$, whereas in CGS units:
$1\text{Jy} = 10^{-23}\text{ergs cm}^{-2}\text{s}^{-1}\text{Hz}^{-1}$. Throughout this work SI units will be used.

The strength of the signal in the discrete case is also referred as the *spectral flux density*, *spectral power flux density* or simply *flux density*. When making an image or a map of a radio source the desired quantity is the spectral flux density per unit solid angle $\text{Wm}^{-2}\text{Hz}^{-1}\text{sr}^{-1}$ and is referred to as *intensity* or *brightness*.

2.3 The Two-Element Interferometer

A large interferometric antenna array configuration can be regarded as a collection of many two-element interferometers. It is therefore very important to have a good knowledge of the concept of the two-element interferometer in order to have a good understanding when generalizing to an array of antennas.

2.3.1 Response of an Interferometer

First we will consider the simple case of monochromatic radiation with frequency f. The interferometer consists of two omnidirectional elements, Antenna 1 and Antenna 2, with a separation distance b. The source is at an angle θ from the normal, which is perpendicular to the interferometer baseline. The voltages produced from the electric fields received by the two antennas are U_1 and U_2, respectively. The radio waves from the source have to travel a longer distance equal to $b \sin\theta$ before it reaches Ant. 2 and therefore the voltage is time delayed by $b \sin\theta / c$, which is called the *geometric delay* τ_g. Expressed in vector form, with the unit vector $\hat{\mathbf{s}}$ pointing towards the source and the baseline vector $\mathbf{b}$ pointing from Ant. 1 to Ant. 2, the geometric time delay becomes $\tau_g = \mathbf{b} \cdot \hat{\mathbf{s}}/c$.

The received signals from a cosmic source can be considered to be a continuous random process and can therefore be represented in the following way:

$$U_1(t) = u_1 \cos(2\pi f t)\,, \tag{2.1}$$

$$U_2(t) = u_2 \cos(2\pi f (t - \tau_g))\,. \tag{2.2}$$

The signals are then multiplied together and averaged. If we assume identical gain on the antennas, the averaged output $r(\tau_g)$ of the multiplier, also known as the *crosscorrelation* [3], will be:

$$r(\tau_g) = u_1 u_2 \cos(2\pi f \tau_g)\,. \tag{2.3}$$

A system consisting of a multiplying device and a time-averaging circuit is referred to as a *correlator*.

The angle θ will change as the source rises and sets and because of that $r(\tau_g)$ will vary in a quasi sinusoidal way, and for this reason $r(\tau_g)$ is called the *fringe* or the *fringe pattern*. The term $u_1 u_2$ is proportional to the received power and represents the fringe amplitude.

The output from the interferometer can furthermore be expressed in terms of the effective area of the antennas A and the source intensity I, both in the direction of the unit vector $\hat{\mathbf{s}}$. The signal power received in the finite bandwidth Δf from a source element $d\Omega$ is $AI\Delta f d\Omega$. The output from the correlator is proportional to the received power and the fringe term:

$$dr = A(\mathbf{s}) I(\mathbf{s}) \Delta f \cos(2\pi f \tau_g)\, d\Omega. \tag{2.4}$$

Expressed in terms of the baseline vector $\mathbf{b}$ and the source vector $\mathbf{s}$, and integrated over the entire celestial sphere S, we can write Eq. (2.4) in the following form:

$$r = \Delta f \int_S A(\mathbf{s}) I(\mathbf{s}) \cos\left(\frac{2\pi f \mathbf{b} \cdot \hat{\mathbf{s}}}{c}\right) d\Omega. \tag{2.5}$$

In the process of synthesizing an image of a source one usually specify a direction of which the field of view is to be centered, most likely in the direction of

maximum antenna gain, referred to as the *phase tracking center* or *phase reference position*. This direction is represented by the vector $\hat{\mathbf{s}}_\mathbf{0}$, and the direction to an element of the source at solid angle $d\Omega$, is then $\hat{\mathbf{s}} = \hat{\mathbf{s}}_\mathbf{0} + \hat{\sigma}$. Equation (2.5) expressed in terms of $\hat{\mathbf{s}}_\mathbf{0}$ and $\hat{\sigma}$ results in:

$$\begin{aligned} r = \Delta f \cos\left(\frac{2\pi f \mathbf{b}\cdot\hat{\mathbf{s}}_\mathbf{0}}{c}\right) \int_S A(\sigma) I(\sigma) \cos\left(\frac{2\pi f \mathbf{b}\cdot\hat{\sigma}}{c}\right) d\Omega \\ -\Delta f \sin\left(\frac{2\pi f \mathbf{b}\cdot\hat{\mathbf{s}}_\mathbf{0}}{c}\right) \int_S A(\sigma) I(\sigma) \sin\left(\frac{2\pi f \mathbf{b}\cdot\hat{\sigma}}{c}\right) d\Omega. \end{aligned} \tag{2.6}$$

It is now appropriate to introduce, one of the most important quantities in synthesis imaging, the *visibility* which is a measure of the coherence from the brightness distribution. The complex visibility is defined as:

$$V = |V| e^{i\phi_V} = \int_S A_N(\sigma) I(\sigma) e^{-2\pi i f \mathbf{b}\cdot\hat{\sigma}/c}. \tag{2.7}$$

where A_N is the reception pattern normalized to the antenna collecting area A_0 in the direction of $\hat{\mathbf{s}}_\mathbf{0}$. The complex visibility, Eq. (2.7), can be separated into its real and imaginary parts:

$$\int_S A_N(\hat{\sigma}) I(\hat{\sigma}) \cos\left(\frac{2\pi f \mathbf{b}\cdot\hat{\sigma}}{c}\right) d\Omega = A_0 |V| \cos\phi_V, \tag{2.8}$$

$$\int_S A_N(\hat{\sigma}) I(\hat{\sigma}) \sin\left(\frac{2\pi f \mathbf{b}\cdot\hat{\sigma}}{c}\right) d\Omega = -A_0 |V| \sin\phi_V. \tag{2.9}$$

Inserting Eqs. (2.8) and (2.9) into Eq. (2.6) gives:

$$r = A_0 \Delta f |V| \cos\left(\frac{2\pi f \mathbf{b}\cdot\hat{\mathbf{s}}_\mathbf{0}}{c} - \phi_V\right). \tag{2.10}$$

The final output of the correlator is then expressed in terms of a fringe pattern, the cosine term in Eq. (2.10), corresponding to a hypothetical point source in the direction of $\hat{\mathbf{s}}_\mathbf{0}$. The complex visibility V in Eq. (2.7) is a fundamental parameter in interferometry, containing the brightness distribution of the source measured in [Jy].

2.3.2 Effect of Bandwidth

The additional time delay, τ_i, has so far been set to zero. That assumption will be relaxed, *i.e.* the signal received by the second antenna lags by the time delay

$\tau = \tau_g - \tau_i$. Eqs. (2.1) and (2.2) can now be expressed in the form:

$$U_1(t) = U(t), \tag{2.11}$$
$$U_2(t) = U(t - \tau). \tag{2.12}$$

The resulting output from the integrator, with a time constant of 2T is:

$$r(\tau) = \frac{1}{2T} \int_{-T}^{T} U(t)U(t - \tau)dt. \tag{2.13}$$

Explained in words; the integrator sums the output from the multiplier for $2T$ seconds after it resets to zero. If the bandwidth, Δf, is small compared to the integration time $2T$, Eq. (2.13) can be written as:

$$r(\tau) = \lim_{T\to\infty} \frac{1}{2T} \int_{-T}^{T} U(t)U(t - \tau)dt. \tag{2.14}$$

Remember that this is only an approximation since $T \to \infty$ is an impossible condition. In terms of signal processing Eq. (2.14) is called the *autocorrelation* function [6].

Fourier analysis is a very important tool in the study of random processes. The cosmic radiation can often be considered as a random process. Hence we can use common mathematical tools, involving Fourier analysis and signal processing.

The *power spectrum* is an important tool when analyzing signals and provides us with a frequency domain description [3]. The spectrum of a signal is the Fourier transform of the autocorrelation function of the same signal.

$$S(f) = \int_{-\infty}^{\infty} C(\tau)e^{-2\pi i f\tau} d\tau, \tag{2.15}$$
$$r(\tau) = \int_{-\infty}^{\infty} S(f)e^{2\pi i f\tau} df. \tag{2.16}$$

In most mapping applications one try to keep the instrumental delay, τ_i, so $\tau = \tau_g - \tau_i$ becomes small, *i.e.* $\tau_g \approx \tau_i$.

2.4 Sensitivity

Sensitivity is one quantity that define the performance of an interferometric array. The sensitivity is a measure of the weakest source that can be detected. The *System Equivalent Flux Density*, I_{S} is a good measure of the sensitivity that takes into account the system noise temperature, the collecting area and efficiency of the antennas.

The antenna noise temperature is given by:

$$T_{\mathrm{a}} = \eta T_{\mathrm{sky}} + (1 - \eta)T_0. \tag{2.17}$$

T_{sky} is the galactic background noise, T_0 is the environmental temperature and η is the radiation efficiency. At frequencies below 400 MHz the galactic background noise is approximately proportional to $\lambda^{2.55}$ [12] and will dominate the antenna noise temperature.

The system noise temperature is then:

$$T_{\text{sys}} = T_{\text{a}} + T_{\text{rec}}, \tag{2.18}$$

where T_{rec} is the receiver noise temperature. It is possible to design a receiver system such that T_{a} is the dominating factor so that T_{rec} can be neglected *i.e.*:

$$T_{\text{sys}} \approx \eta T_{\text{sky}}. \tag{2.19}$$

The collecting effective area is defined as:

$$A_{\text{e}} = \frac{\lambda^2}{4\pi} G. \tag{2.20}$$

The gain G is equivalent to the maximum directivity D if the antenna losses are neglected. Hence, the maximum effective area for a lossless antenna is:

$$A_{\text{em}} = \frac{\lambda^2}{4\pi} D. \tag{2.21}$$

The above relationships leads to the system equivalent flux density:

$$I_{\text{S}} = \frac{2 T_{\text{sys}} \text{k}_{\text{b}}}{A_{\text{em}}}. \tag{2.22}$$

The system equivalent flux density is derived for one antenna and does not take into account the time of observation nor the bandwidth. The root mean square noise power flux density ΔI_{S}, derived in [1], relates the system equivalent flux density to the bandwidth Δf of the array and the time of integration. The expression for an array with N identical antenna elements is:

$$\Delta I_{\text{S}} = \frac{I_{\text{S}}}{\eta_s \sqrt{N(N-1)\Delta f \Delta t_{int}}}. \tag{2.23}$$

Here η_s is the system efficiency factor and accounts for various losses in the electronics and digital equipment.

Eq. (2.23) is the sensitivity for a single polarization image. If dual polarization data with ΔI_S per polarization are available the sensitivity of an image changes as:

$$\Delta I_S \rightarrow \frac{\Delta I_S}{\sqrt{2}}. \tag{2.24}$$

If three polarizations are available:

$$\Delta I_S \rightarrow \frac{\Delta I_S}{\sqrt{3}}. \tag{2.25}$$

In principle, if we were able to make comparable measurements of both the three-dimensional electric and the magnetic field vectors $\bar{E}(\bar{x}, t)$ and $\bar{B}(\bar{x}, t)$, respectively a sensitivity of:

$$\Delta I_S \rightarrow \frac{\Delta I_S}{\sqrt{6}}, \tag{2.26}$$

could be obtained.

2.5 Resolution

The angular resolution of an antenna array radio telescope is determined by its size and the observed wavelength, and works essentially like a single dish telescope with diameter equal to the arrays maximum baseline. Approximately it is:

$$\lambda/|\mathbf{b}|_{max}. \tag{2.27}$$

Chapter 3

Geometrical Relationships

3.1 Background

The fundamental equations in interferometry were introduced in Ch. 2. For practical use, two right-handed coordinate systems *(u,v,w)* and *(l,m,n)* are employed to express the interferometer baseline and the source brightness distribution. A more rigorous derivation on how to obtain the u,v data from an array of antennas is covered in the following section.

3.2 The visibility function in (u,v,w) coordinates

The *(u,v,w)* coordinates are expressed in wavelength with w in the direction of the phase tracking center $\hat{\mathbf{s}}_\mathbf{0}$, and *(u,v)* towards East and North, respectively. The *(l,m)* coordinates represent positions on the celestial sphere with origin at the phase tracking center and are direction cosines measured with respect to u and v. To express the visibility function in these coordinate systems the following terms are derived:

$$\frac{f\mathbf{b}\cdot\hat{\mathbf{s}}}{c} = ul + vm + wn, \tag{3.1}$$

$$\frac{f\mathbf{b}\cdot\hat{\mathbf{s}}_\mathbf{0}}{c} = w, \tag{3.2}$$

$$d\Omega = \frac{dldm}{n} = \frac{dldm}{\sqrt{1-l^2-m^2}}. \tag{3.3}$$

Hence Eq. (2.7) becomes:

$$V(u,v,w) = \int_{-\infty}^{\infty}\int_{-\infty}^{\infty} A(l,m)I(l,m)e^{-2\pi i(ul+vm+w(\sqrt{1-l^2-m^2}-1))}\frac{dldm}{\sqrt{1-l^2-m^2}}. \tag{3.4}$$

This fundamental relationship between the visibility and the source distribution is the basis of radio interferometry. In the optical literature it is also referred to as the Van Cittert-Zernike theorem [18].

Equation (3.4) can be reduced to the form of a two-dimensional Fourier transform if the field of view is small, *i.e.* close to the phase tracking center. The visibility function is then reduced to:

$$V(u,v) = \int_{-\infty}^{\infty}\int_{-\infty}^{\infty} A(l,m)I(l,m)e^{-2\pi i(ul+vm)}dldm. \tag{3.5}$$

In practise, it is the visibility that is the measured quantity, or the output from the correlator. Then by taking the inverse Fourier transform of the visibility the sky brightness or intensity is obtained.

$$A(l,m)I(l,m) = \int_{-\infty}^{\infty}\int_{-\infty}^{\infty} V(u,v))e^{-2\pi i(ul+vm)}dudv. \tag{3.6}$$

3.3 Antenna Baselines in *u,v,w* coordinates

The visibility function Eq. (3.5) contains the data expressed in the u,v space, therefore we must introduce several conversions so that we can relate the antenna baselines on the ground to a set of points in the u,v space.

The antennas on the ground can be expressed by the direction coordinates East, North, and Zenith *(E,N,Z)*. These coordinates are relative to the local horizon and will change depending on where we are on Earth. In astronomy it is convenient to use a coordinate system aligned with Earth's rotational axis *(x,y,z)*. The transformation matrix between *(E,N,Z)* and *(x,y,z)* is given by:

$$\begin{bmatrix} x \\ y \\ z \end{bmatrix} = \begin{bmatrix} 0 & -\sin\alpha & \cos\alpha \\ 1 & 0 & 0 \\ 0 & \cos\alpha & \sin\alpha \end{bmatrix} \begin{bmatrix} E \\ N \\ Z \end{bmatrix}, \tag{3.7}$$

where α is the latitude on where the antennas are located. Between every possible pair of antennas a baseline vector can formed:

$$\mathbf{b} = (b_x, b_y, b_z) = (x_2 - x_1, y_2 - y_1, z_2 - z_1). \tag{3.8}$$

The interesting parts of the baseline vector are the components perpendicular to the phase tracking center $\hat{\mathbf{s}}_\mathbf{0}$. The following transformation expresses the u,v,w coordinates in terms of hour angle, h_0, and declination, d_0:

$$\begin{bmatrix} u \\ v \\ w \end{bmatrix} = \frac{1}{\lambda} \begin{bmatrix} \sin h_0 & \cos h_0 & 0 \\ -\sin d_0 \cos h_0 & \sin d_0 \sin h_0 & \cos d_0 \\ \cos d_0 \cos h_0 & -\cos d_0 \sin h_0 & \sin d_0 \end{bmatrix} \begin{bmatrix} b_x \\ b_y \\ b_z \end{bmatrix}. \tag{3.9}$$

The wavelength λ corresponds to the center frequency of the receiving system.

3.4 Geometric definitions between antenna positions on ground and in orbit

For advanced antenna configurations, in order to obtain high spatial resolution and sufficient sensitivity, it will be needed to place antennas on the ground combined with antennas in orbit. To relate the positions of the antennas to each other at different times, a common geometric coordinate system connecting the antennas is convenient to use. The coordinates for the antennas will be transformed to a Cartesian coordinate system with origin at the center of the celestial body, *e.g.* Earth or Moon, that the antennas are located on.

3.4.1 Antennas on the surface

The antennas on the surface can be positioned using only two parameters, θ and ϕ, equivalent to latitude and longitude on Earth, see Fig 3.2. The third variable is the radius of the body which is fixed for a certain point on the surface specified by θ and ϕ. For simplicity we will assume that the body is a perfect sphere. Hence, all points on the surface have the same distance to the center. The spherical coordinates are then transformed to Cartesian coordinates through the transforms:

$$\begin{cases} x = r \sin\theta \cos\phi \\ y = r \sin\theta \sin\phi \\ z = r \cos\theta \end{cases} \tag{3.10}$$

3.4.2 Antennas in orbit

Representing the antennas in orbit is a bit more complicated. First of all the orbit of the satellite carrying the antenna must specified. All coordinates will be related to a Cartesian coordinate system with origin at the center of the celestial body, with x and y forming a plane through the equator and z in the direction of the spin axis. In a celestial coordinate system x is in the direction of the vernal equinox and y completing the right-handed system. Imagine the sphere in Fig. 3.2 as the celestial body. To represent the orbit five parameters are needed, those are defined as following:

Semimajor Axis: Defining the size of the orbit.

Eccentricity: Defining the shape of the orbit.

Inclination: The angle from the spin axis to the plane through the orbit.

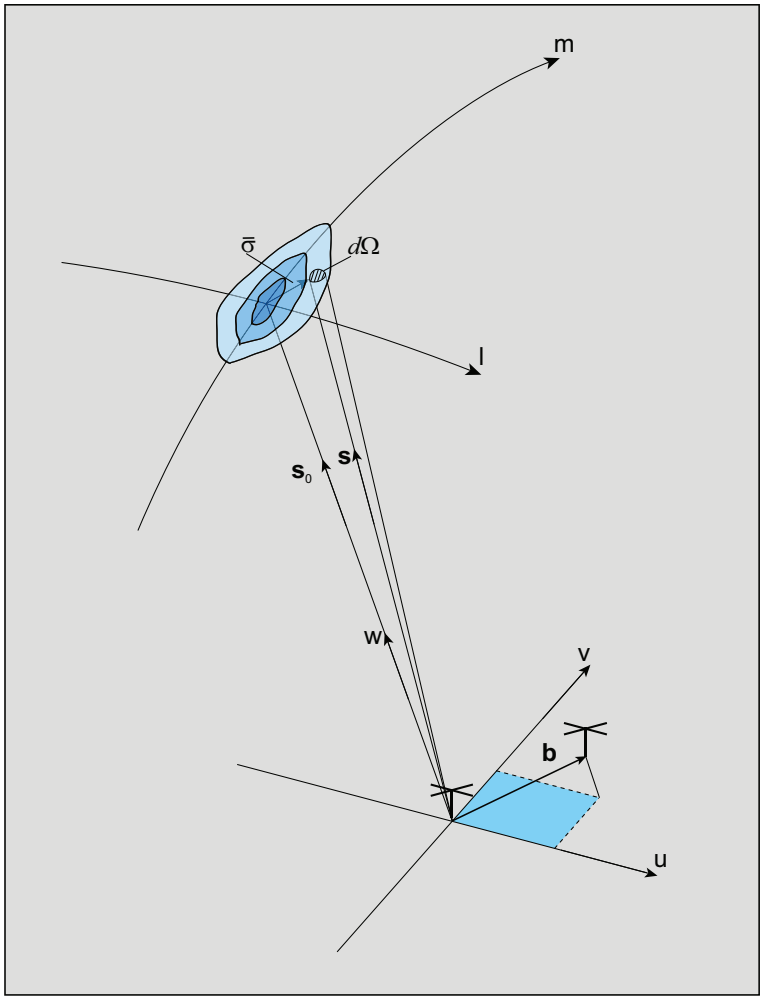

Figure 3.1: The geometric relationship between the source under observation $I(l, m)$, and an antenna pair with baseline b_λ, measured in wavelengths and componetns (u, v, w).

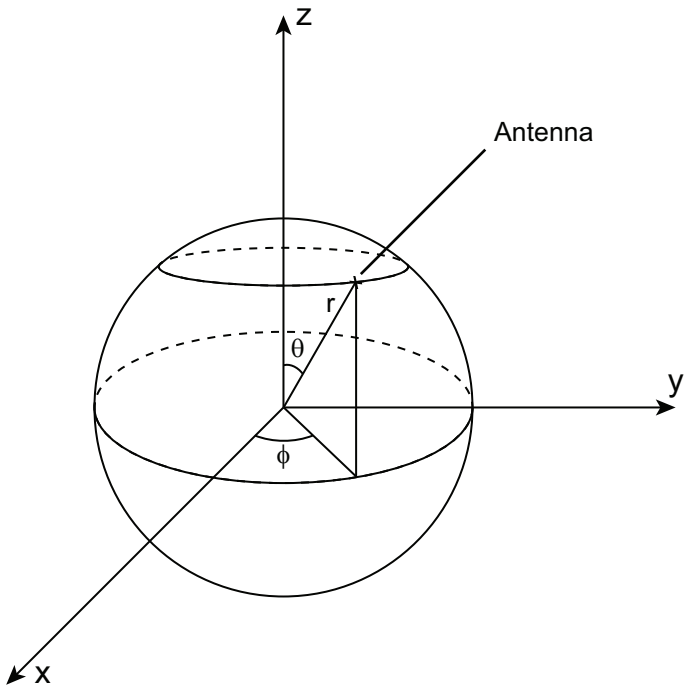

Figure 3.2: The relationship between spherical coordinates representing the antennas and (x,y,z)

Right ascension of the ascending node: The angle from the vernal equinox to the ascending node. The ascending node is the point where the satellite passes through the equatorial plane moving from south to north,.

Argument of perigee: The angle from the ascending node to the eccentricity vector measured in the direction of the satellite's motion. The eccentricity vector points from the center of the celestial body to perigee with a magnitude to the eccentricity of the orbit.

For a more complete picture see SMAAD [3]. Obtaining the position of a satellite at a give time t can be achieved by solving an equation relating the true anomaly ϑ, which is the angle to the satellite from perigee, to the mean anomaly ζ and the eccentric anomaly ξ, see Fig. 3.3. By definition the mean anomaly is:

$$\zeta - \zeta_0 = n(t - t_0), \tag{3.11}$$

where ζ_0 is the mean anomaly at time t_0 and n is the mean motion defined as:

$$n = \left(\frac{G_\mu}{a^3}\right)^{1/2}. \tag{3.12}$$

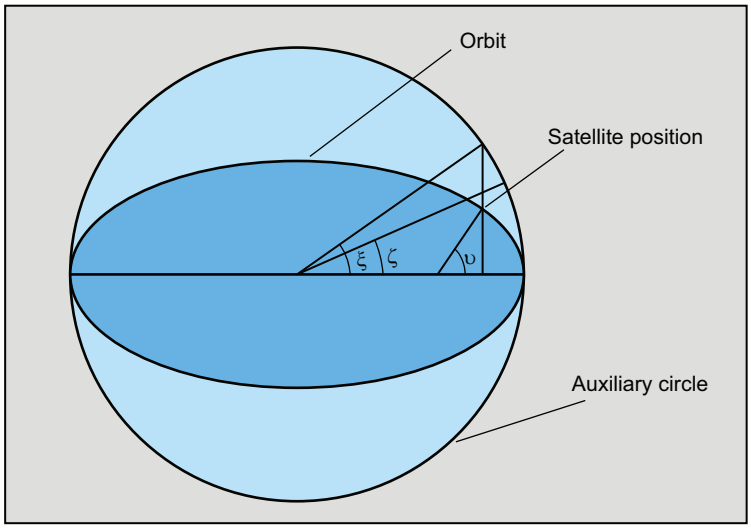

Figure 3.3: The relationship between the true anomaly and the mean and eccentric anomaly

Here G_μ is the celestial body's gravitational constant and a is the length of the semimajor axis. The mean motion and mean anomaly only give the average position and velocity, but in an elliptic orbit the velocity of the satellite depends on its position and varies as the radius change. Here the second auxiliary angle ξ combined with ζ form Kepler's equation:

$$\zeta = \xi - \mathrm{e}\sin(\xi), \tag{3.13}$$

where e denotes the eccentricity of the orbit. Using trigonometric identities the true anomaly can be expressed in terms of ξ:

$$\tan\left(\frac{\vartheta}{2}\right) = \sqrt{\frac{1+\mathrm{e}}{1-\mathrm{e}}}\tan\left(\frac{\xi}{2}\right) \tag{3.14}$$

This is a transcendental equation. Therefore, to find the eccentric anomaly Eq. (3.13) must be solved using an iterative method. After acquiring the true anomaly at time t the magnitude of the position vector to the ellipse is obtained by inserting ϑ in:

$$r = \frac{a(-\mathrm{e}^2)}{1+\mathrm{e}\cos\vartheta}. \tag{3.15}$$

The satellite position at any given time can now be calculated. Basically the true anomaly ϑ provide the information for determining the position in the elliptical orbit, and through the five orbital parameters the orbit itself can be described.

3.5 Antenna Configurations

Each pair of antennas, in an antenna array configuration, forms a baseline. An array consisting of n_a antennas then contains a number of baseline equal:

$$N_\mathrm{a} = \frac{n_\mathrm{a}(n_\mathrm{a} - 1)}{2}. \tag{3.16}$$

The primary concern when constructing an antenna array configuration is how to optimize the sampling of the visibility function. Remember that we inverse Fourier transform the visibility, Eq. (3.5), to obtain the brightness distribution or intensity, Eq. (3.6), of the observed region of the sky.

Each antenna is forming correlations with all $n_\mathrm{a} - 1$ other antennas, providing us with a total of approximately n_a^2 correlations. In the *(u,v)* space those correlations are represented by the tips of each baseline vector, and all baseline vectors together will place tips on the rectangular *(u,v)* grid forming the *coverage*, which represent the sampling of the visibility. This results in a snapshot of the coverage, then by using aperture synthesis methods (briefly explained in Sec. 2.2) a larger aperture can be synthesized.

A commonly used configuration is the East-West linear array, as illustrated by the left panel in Fig. 3.4. As can be seen in the middle panel in Fig. 3.4 the antennas trace out elliptical loci as Earth rotate, filling the *(u,v)* plane. Many famous radio telescopes use this configuration, like the One-Mile Telescope in Cambridge and the Westerbork Synthesis Radio Telescope in northeastern Netherlands. In Figs. 3.5–3.8 a few other configurations are demonstrated. The Cross-array and T-array, Figs. 3.5 and 3.6 respectively, produce similar snapshot coverage's, which implies that in practice the T-array is more often constructed. In 1954 the first Cross array telescope, Mills Cross, was constructed using this technique. The Very Large Array in New Mexico use the Y-shape, Fig. 3.7, configuration and LOFAR, under construction in the Netherlands, use the spiral form showed in Fig. 3.8.

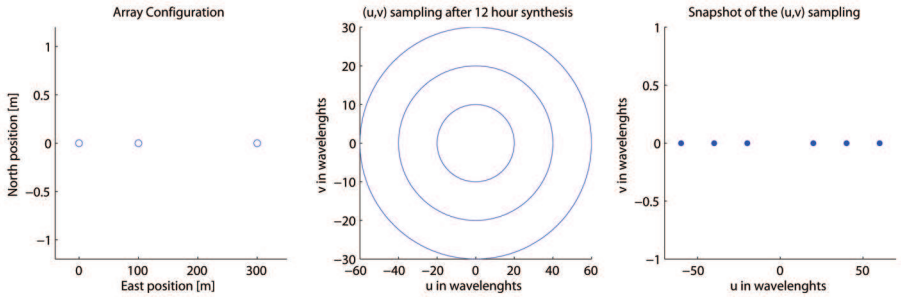

Figure 3.4: An East-West configuration consisting of 3 uniformly spaced antennas at 45° latitude, observing a target at 30° declination

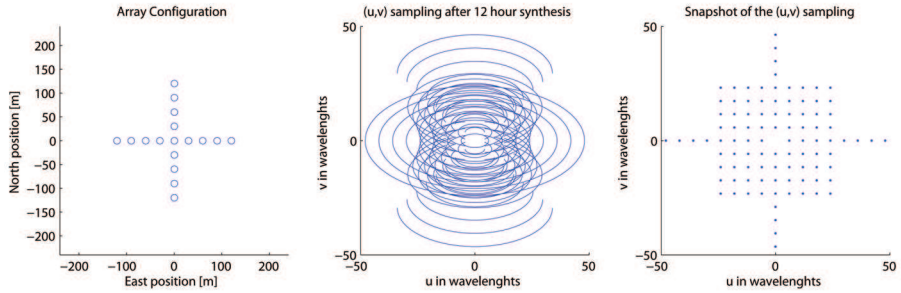

Figure 3.5: A Cross configuration consisting of 17 uniformly spaced antennas at 45° latitude, observing a target at 30° declination

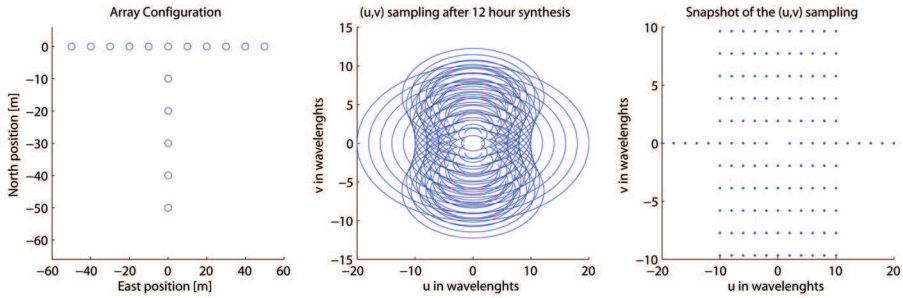

Figure 3.6: A T-array configuration consisting of 16 uniformly spaced antennas at 45° latitude, observing a target at 30° declination

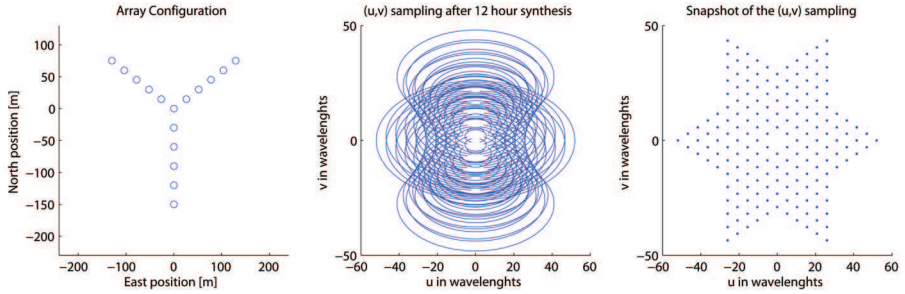

Figure 3.7: An Y-array configuration consisting of 16 uniformly spaced antennas at 45° latitude, observing a target at 30° declination

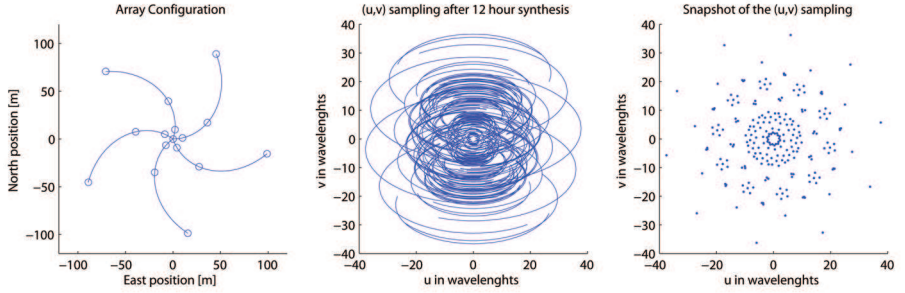

Figure 3.8: A logarithmic spiral configuration consisting of 16 uniformly spaced antennas at 45° latitude, observing a target at 30° declination

Chapter 4

Extrasolar Planet Detection

4.1 Background

Extrasolar planet detection is a rather new branch in astronomy and space physics, mainly due to the difficulties to detect them. Planets are extremely small and faint objects comparing to their host stars, which makes extrasolar planets impossible to spot with today's technology. Instead the scientists have come up with methods to detect them in other ways then direct observations. In this chapter the most common methods used today in the search for extrasolar planets will be presented.

In the future, space based missions will be able to detect extrasolar planets directly using advanced techniques to reduce the starlight, thus enabling detection of the very faint planets. But those kind of missions still have years ahead before they are realized in practice.

Instead of looking at visible wavelength another method has drawn some attention, which try to detect extrasolar planets by their radio emissions. This is a very promising method because the radio emissions might be detectable by already constructed radio telescopes or telescopes under construction, like LOFAR. Direct detection methods of extrasolar planets are superior to indirect methods because they can extract much more information about the physical properties of the planet. Furthermore, direct detection of extrasolar planets would also greatly contribute to planetary science, which is mostly based on observations in our own solar system.

In this chapter the most common methods used today in the searches for extrasolar planets will be presented, then the detection method based on planetary radio emissions will be discussed, and finally a short overview on how the next generation of low frequency radio telescopes can look like.

4.2 Present state of extrasolar planet detection

The first detection of an extrasolar planet was made in 1992 by timing observations of the pulsar PSR1257+12. A pulsar is a rotating dead star that emits radio pulses at extremely regular intervals. Deviations in the regularity of the radio pulses have been used to predict the presence of three planets.

The first detection of a planet orbiting a main sequence star, 51 Peg, was made in 1995 using a different technique, which observe the wobble the planet inflict on the star. This method, called the radial velocity measurement technique, is the most successive method so far and have been used to detect 198 out of totally 210 detected planets as of October 30, 2006. In Fig. 4.1 the most common and successful indirect methods for extrasolar planet detection are listed together with short descriptions.

The methods mentioned above are indirect techniques of planetary detection, *i.e.* they observe the host star and planets are detected from discrepancies in its behavior. As a consequence the observable properties of the planet are limited, for example the radial velocity measurement technique, also known as doppler shift method or radial velocity method, can only measure the minimum mass and some orbital parameters, and with today's technology it is only possible to detect huge gas giants which are extremely close to their host star. To get a more complete characterization of a planet, direct methods are needed. The first image of an extrasolar planet was announced in April 2004. The European Southern Observatory's (ESO) Very Large Telescope (VLA) detected a faint object close to a brown dwarf known as 2M1207A. Follow-up observations with the Hubble telescope confirmed what is truly an orbiting companion to the brown dwarf.

Since the first direct image of an extrasolar planet three more planets have been detected directly. Those are very massive planets, at least 5 Jupiter masses, and very far from their stars, closest with a semimajor axis on 46 AU. To detect smaller planets more sensitive telescopes are needed or new methods most be developed. A brief summary of future mission can be found in Sec. 5.2.

4.3 Non-thermal radio emission

In our own solar system, planets with magnetic fields produce intense non-thermal cyclotron radio emissions. The radiation originates from the interaction between a planetary magnetic field and a source of energetic electrons, such as a stellar wind.

When the energetic electrons propagate along the magnetic field lines into the auroral region electromagnetic emissions are produced, known as auroral emissions or northern lights in the visible region. A part of the solar wind power is converted into escaping cyclotron radio emissions, which have a frequency that is directly proportional to the magnetic field strength of the planet. Detection of radio emissions from an extrasolar planet would be a direct detection and the presence of a magnetic field provides a rough measure of the composition of the planet.

4.3.1 The Radiometric Bode's Law

The cyclotron emissions are in general created in the auroral regions at one to three planetary radii in altitude. The power emitted differ from planet to planet, depending for instance on the atmospheric densities, magnetic field topology and solar wind power. Still, a general relationship relating the incident solar wind power to the median emitted radio power is applicable and is sometimes called the "radiometric Bode's law",

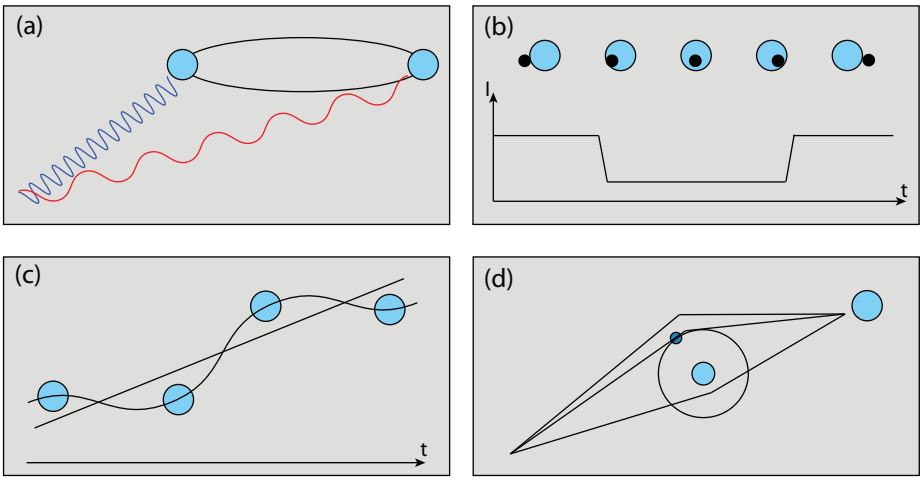

Figure 4.1:

(a) **Doppler shift method**: This method, also known as radial velocity method, measures the Doppler shifts in the spectral lines of the star's spectrum. Planets orbiting a star will cause it to wobble. The spectral lines will be red shifted when the planet is moving away from us and blue shifted when the planet is approaching us.

(b) **Transit**: This metod use the fact that when an object passes in front of a star its luminosity is decreased. This is a promising method that can be able to detect Earth sized planets and even the atmospheric composition as well as orbiting moons.

(c) **Astrometry**: This is an old method that measure the wobble that a planet induce upon a star. Up to date only one planet has been detected using this method. Still it have a promising future in the GAIA and SIM space missions, both using astrometry for extrasolar planet detection.

(d) **Microlensing**: A promising new method is the microlensing method. It's a phenomenon that occur when an object with enough mass passes between us and a distant background star. The planet star system acts like a lens and bends the light from the background star, hence increase its apparent luminosity.

$$P_{\rm rad} = \epsilon P_{\rm sw}^{x}, \tag{4.1}$$

where $P_{\rm rad}$ is the median emitted radio power, $P_{\rm sw}$ is the incoming solar wind power, $\epsilon \sim 10^{-5} - 10^{-6}$ is the efficiency of how much of the solar wind power is converted into emitted radio power, and exponent $x \approx 1$. The measurements of ϵ and x depend on available data and have therefore fluctuated historically. The first estimate was evaluated from data based on Jupiter and Saturn fly-by's, and later including fly-by's of Uranus and Neptune.

Blackett (1947) derived a formula that related a planet's magnetic moment to its rotation rate ω and mass M by:

$$\mu \sim \omega M^2. \tag{4.2}$$

Combining various scaling factors with the above mentioned Eqs. (4.1) and (4.2) Farell *et al.* (1999) and Zarka *et al.* (2001) extrapolated the radiometric Bode's law to extrasolar planets:

$$P_{rad} \sim 4 \times 10^{11} W \left(\frac{\omega}{10hr}\right)^{0.79} \left(\frac{M}{M_J}\right)^{1.33} \left(\frac{d}{5AU}\right)^{-1.6}. \tag{4.3}$$

The quantities are normalized to those of Jupiter. The characteristic emission frequency can be related to the planetary magnetic dipole moment by:

$$f_c \sim 23.5 \left(\frac{\omega}{\omega_J}\right) \left(\frac{M}{M_J}\right)^{5/3} R_J^3 [MHz]. \tag{4.4}$$

Combining Eqs. (4.1)–(4.4) the predicted flux densities of an extrasolar planets can be derived using the following equation.

$$I = \frac{P_{\rm rad}}{\Delta f \Omega D^2}. \tag{4.5}$$

Here Ω is the emission cone, Δf the bandwidth and D the distance to the extrasolar planetary system.

4.4 Radio detection of known extrasolar planets

The first step to test, if detection of radio emission from extrasolar planets is possible, should be to detect the extrasolar planets that have already been detected by means of the indirect methods mentioned in section Sec. 4.2. This has been performed with the VLA telescope in New Mexico but without success.

The frequencies observed by VLA are 1465 MHz, 333 MHz and 74 MHz with typical sensitivities 0.02-0.07 mJy at 1465 MHz, 1-10 mJy at 333 MHz and $\sim$ 50 mJy at 74 MHz. We will later in this section show that those sensitivities are probably not sufficient to detect extrasolar planets.

Using Eqs. (4.1)–(4.5) make it possible to calculate the predicted flux densities from extrasolar planets, and by taking data from observations of known extrasolar planets we can predict the flux densities for those planets. The vast majority of the planets have been discovered by using the radial velocity method, which only provide the minimum mass of the planet and orbital parameters like

Planet	D[pc]	M_J	d[AU]	T[days]	ω/ω_J	f_c[MHz]	$\log(I)$	$\log(P_{\rm rad})$
HD 189733 b	19.3	1.15	0.031	2.22	0.19	10.88	-2.75	14.64
HD 73256 b	36.5	1.87	0.037	2.55	0.16	21.30	-3.48	14.75
Tau Boo b	15.0	3.90	0.046	3.31	0.13	55.77	-2.94	14.93
HD 162020 b	31.3	13.75	0.072	8.43	0.05	179.07	-3.99	15.03
55 Cnc b	13.4	0.78	0.115	14.67	1	30.60	-3.43	14.08
HD 192263 b	19.9	0.72	0.150	24.35	1	26.55	-3.95	13.85
Gliese 876 b	4.7	1.94	0.208	60.94	1	137.91	-3.07	14.19

Table 4.1: Extrasolar planets within LOFAR's frequency range and strong flux densities.

semimajor axis, eccentricity and orbital period. To calculate the flux densities a few assumption must therefore be made.

In Eq. (4.3) the rotation rate ω is unknown. For a planet that is closer then 0.1 AU to its host star, the planet is assumed to be tidally locked, *i.e.* it has the same rotation rate as the orbital period. If the distance is greater then 0.1 AU the planets is assumed to have the same rotation period as Jupiter, which is approximately 10 hours. This is based on the periods of our solar system. The 10 h rotation is normalized to Jupiter but Saturn, Neptune and Uranus have respectively 11 h, 16 h and 17 h which means that it is a possible assumption. Mercury, the closest planet to the Sun, is not tidally locked but rotates three times every two orbits around the Sun. With today's science in planetary formation those assumptions are probable.

In Eq. (4.4), when calculating the characteristic frequency, tidally locked planets are assumed to have a radius of $1.25R_J$, based on observations of the planet orbiting HD 209458 [16]. Finally, when using Eq. (4.5) to calculate the flux density, the emission cone Ω is assumed to be 4π sr and $\Delta f = f_c/2$.

In the "*Extra Solar Planets Encyclopaedia*" Jean Scneider is listing all detected extrasolar planets. Of the 209 planets (Jan 8, 2007) listed in the encyclopedia, 197 of them has been detected using the radial velocity method. From this set planets closer than 40 pc from our solar system were selected and used when calculating the predicted flux densities in App. B.

Radio detection with LOFAR

The aim of this research is to investigate the possibility to detect radio emissions from extrasolar planets. It is therefore very interesting to see if LOFAR will be able to detect them. From all 121 planets listed in App. B, those within LOFAR's frequency range and with strong flux densities were selected. I ended up with seven candidates see Tab. 4.4. The flux densities stretches from $-2.75 = 1.8$ mJy at 11 MHz to $-3.99 = 0.1$ mJy at 180 MHz. LOFAR, observing 1 hour with a single polarization, can achieve sensitivities as high as 3.0 mJy at 10 MHz and about 0.03 mJy at 200 MHz. Those values are close to those needed to detect the extrasolar planets in Tab. 4.4, but LOFAR can handle dual polarization data and using longer observation times all those planets should definitively be detectable.

4.5 Detection of Earth sized planets

Almost all planets listed in App. B are heavy gas giants of the size of Jupiter or larger. An interesting thought is if Earth sized planets can be detected with this method. Unfortunately, using the equations derived in Sec. 4.3 results in characteristic emission frequencies in the orders of a few kilohertz. Building telescopes at those wavelength with sufficient sensitivities are unfeasible. On the other hand the equations relay on empirical observations in our solar system, and mainly on the big gas giants, implying that the various scaling relationships may not be correct for smaller planets. Observations show that Earth emits in frequencies up to 800 kHz [19], confirming that those equations are not accurate for smaller planets. Building antenna arrays observing at frequencies around 1 MHZ is possible; thus Earth sized planets could be detectable by looking at their radio emissions.

The first step is to see if it is possible to detect already detected extrasolar planets. To determine if Earth size planets can be detected, more research in the field of planetary radio emission, is needed.

4.6 Moon Array

A major problem with detection of radio emissions from extrasolar planets lies at the heart of Eq. (4.4). The characteristic emission frequency is proportional to, or almost, the mass squared, implying that planets smaller then the size of Jupiter will emit in frequencies below the ionospheric cut-off, which is around 10 MHz. An Earth based telescope can therefore impossibly be used for such detections. The alternative is to construct a telescope above Earth's ionosphere. Free-flyers can be an option, but due to the amount of antennas and the necessity of supercomputers to handle the signal processing, such a formation will probably be hard to control and maintain, if the number of antennas become more then a few hundred. This is not a problem I have investigated deeply, I only mention difficulties that can arise, not if it is possible or not. Instead I will discuss another option of placing a telescope in space, more precisely, building an array on the Moon's surface, and combine them with free-flyers to improve the performance.

Some of the difficulties with low frequency measurements are the sensitivity and the spatial resolution. The resolution, Eq. (2.27), for a fixed wavelength can only be improved by increasing the baseline. This is a big issue at low frequencies when the wavelengths are in intervals from meters up to kilometers. It is also difficult to achieve high sensitivity, Eq. (2.23), due to the antenna noise temperature, which is approximately proportional to $\lambda^{2.55}$ at low frequencies. To improve the sensitivity, more antennas can be added, taking observations for longer periods of time, or averaging many different observations. Using broader bandwidth can also enhance the sensitivity.

Using the basic concepts of interferometry derived in Ch. 2 and the geometrical relationships derived in Ch. 3 a few scenarios on how such a telescope could be constructed, including a configuration solving some of the mentioned issues, have been simulated.

In Fig. 4.6 the basic ideas of a Moon array are illustrated. Using the far side has the advantage that the Moon itself block all radio emissions from Earth.

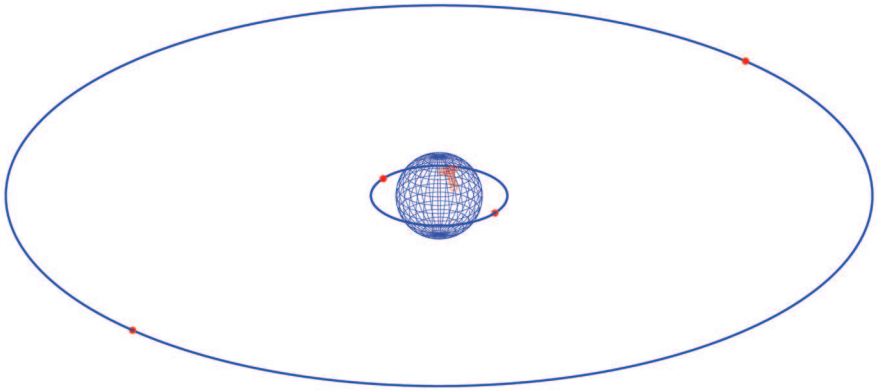

Figure 4.2: Concept design of an array located on the Moon combined with antennas in orbits.

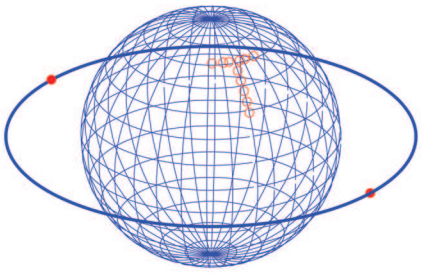

Figure 4.3: A magnified picture illustrating the array located on the surface with the closest orbit.

Hence, only cosmic radiation will be received by the interferometer. But placing them there also complicate the transmission of the data back to Earth. Adding more antennas in orbit can be a good way to solve this problem because a link, between the antennas on the surface via satellites, to Earth can be maintained. Placing antennas in orbits will dramatically increase the spatial resolution due to longer baselines and the extra antennas will also improve the sensitivity of the array.

Chapter 5

Concluding Remarks

5.1 Lunar Observatories

The Moon array discussed in Section 4.6 seems to be an impossible project, to big and to expensive, but actually the idea of building a telescope on the Moon is a thought shared by many scientist around the world.

In November 2006 I attended, accompanied by my supervisor Jan Bergman and a few others, a workshop in Bremen called "*Towards a European Infrastructure for Lunar Observatories II*" with main goal to inform the scientific community about the current status of a European lunar observatory, and to provide a timely input in the programmatic discussion in preparation for the ESA Ministerial Council in 2008. The possibility of building a telescope on the Moon have become viable since more and more nations are turning there attention to space. NASA and ESA have, in there strategic documents, included human missions to both the Moon and Mars. This may open up opportunities for scientific applications and make a lunar observatory become a reality.

The workshop was the second in order and the group has already come up with concept designs for lunar missions. ASTRIUM (formerly EADS) Space Transportation in Bremen designed a concept called LIFE "Lunar Infrastructure For Exploration" which should be a supporting platform for scientific and logistics demands and missions. Using LIFE they have also designed an entry mission using LOFAR technology to establish a radio telescope with a diameter of several 10s of kilometers using a single Ariane 5 launch. An illustration of the mission is shown in Fig. 5.1.

The workshop resulted in a joint statement signed by all participants, including a general statement, statements on science goals and potential observatories, and statements on technical issues [13].

ELVIS is another project created by Jan Bergman at the Swedish Institute of Space Physics and have team members in USA, Netherlands, UK, Finland, Austria and France as well. The ELVIS project has scientific objectives in three major fields including lunar and solar wind space plasma physics, radio astronomy, and astroparticle physics. Investigation of the electromagnetic environment in radio frequencies around the Moon gives the opportunity to perform research in a field never touched before, and using the Moon itself as a target, ultra-high energy cosmic rays and neutrinos interacting with the lunar surface

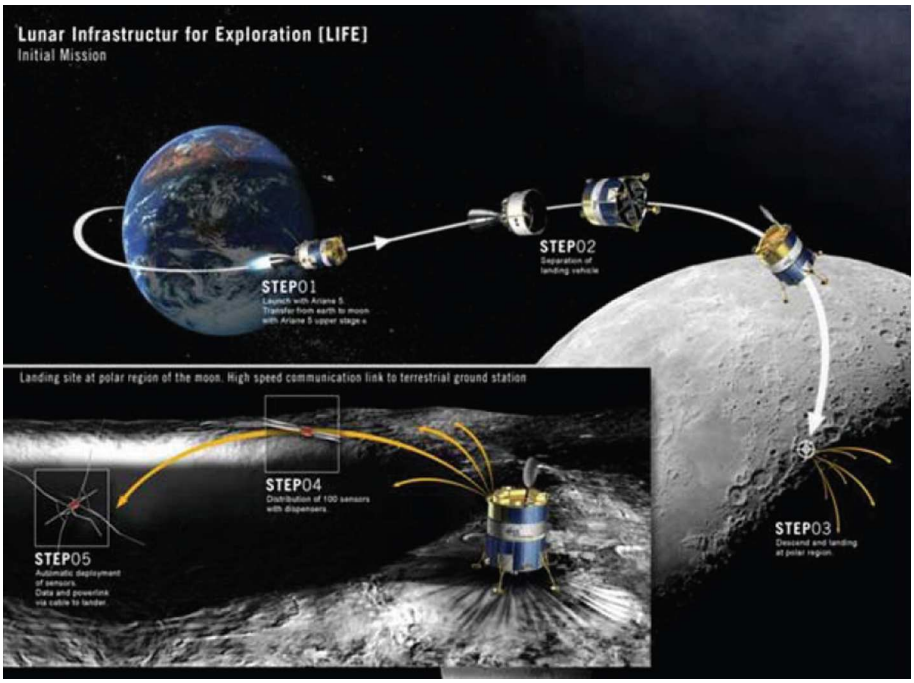

Figure 5.1: A concept design illustrating how to place an antenna array on the Moon's surface.

layer can be detected.

ELVIS will make use of a total number of 80 spacecrafts arranged in 5 clusters with 16 satellites in each. Those satellites could be connected with a LOFAR like antenna array on the Moon's surface and realize the Moon array discussed in Sec. 4.6.

On Feb 2, 2007, NASA came up with a list of potential lunar objectives called "181 Things To Do On the Moon" [15]. The number one objective is to perform radio astronomy on the far side of the Moon. They summarize it as follow: "Radio interferometry antenna arrays, as well as single dish antennae, located on the far-side of the Moon could provide data on exotic phenomena in the universe: pulsars, black holes, planetary radio emissions, and the remnants of the Big bang." NASA also state that they plan to send astronauts to the Moon no later then 2020.

Many nations and space agencies have plans on missions to the Moon. Building a radio telescope there is a big project but the scientific output seems to justify it.

5.2 Future projects for Extrasolar Planet Searches

Vast amounts of money is being invested in extrasolar planet searches. NASA have several projects in the planning stage, using both indirect and direct methods. In this section a few of them will be described.

Mission	Launch Date	Detection Method	Detection Limit	Cost
Kepler	2008	Transits	Earth Mass	$300 000 000
SMI	2010-2019	Astrometry	Earth Mass	>$300 000 000
TPF	2014/2020	Direct Imaging	Mars Mass	$2-4 000 000 000

Table 5.1: Summary of three NASA missions for extrasolar planet detection

Kepler Mission

The scientific objective of the Kepler Mission is to explore the structure of planetary systems by surveying a large number of stars. Kepler looks for transits *i.e.* it looks at changes in star brightness. When a planet transits the disk of its star the telescope onboard Kepler can measure changes in the brightness distribution. Depending of the change in brightness and the transit time the size and orbit parameters of the planet can be determined.

Kepler is scheduled for launch in October 2008 and will in addition to its primary task make way for future missions by identifying common stellar characteristics of host stars and defining the volume space needed for other projects.

Space Interferometry Mission, SIM

The Space Interferometry Mission (SIM) scheduled for launch at some point in the next decade, is a powerful telescope using two mirrors collecting light and combining them through interferometry. The detection of extrasolar planets is performed by observing the wobble in the host star's apparent motion. The accuracy of the telescope is enough to detect Earth sized planets, but it is still based on indirect detection, which means that no more information then the mass and orbital parameters can be determined.

Terrestrial Planet Finder (TPF)

The Terrestrial Planet Finder (TPF), is the first space-based mission for direct detection of extrasolar planets. The telescope consist of two complementary observatories. The first, planned to be launched in 2014, working at optical wavelengths and the second, planned to be launched in 2020, working as an infrared interferometer. Together they will be able to detect Earth sized planets and determine their size and temperature, and with the onboard spectroscope the atmospheric composition can be measured.

Acknowledgements

I would like to than my supervisor Jan Bergman for his devotion to the subject of my thesis. He has encourage me and helped me through my work and he has also given me opportunities to meet the scientific frontier in low frequency radio astronomy which has been a great experience.

I would also like to thank Lars Daldorff for his involvement in my thesis, for the help and for the support.

Last, but not least, I would like to thank all the diploma workers on the Institute of Space Physics and the Signals and Systems group for all their support and for the great time we had together.

Appendix A

Derivations

A.1 Calculation of the two-element output

The output of the two-element interferometer is a multiplication of the voltages on each antenna:

$$U_1(t) = u_1 \cos(2\pi f t), \tag{A.1}$$
$$U_2(t) = u_2 \cos(2\pi f(t - \tau_g). \tag{A.2}$$

A complete derivation of the multiplication using trigonometric formulas is performed below:

$$\begin{aligned} U_1U_2 &= \cos(2\pi f t)\cos(2\pi f(t-\tau_g) \\ &= \cos(2\pi f t - 2\pi f(t-\tau_g)) + \cos(2\pi f t + 2\pi f(t-\tau_g)) \\ &= \cos(2\pi f \tau_g) + \cos(4\pi f t - 2\pi f \tau_g) \\ &= \cos(2\pi f \tau_g) + \cos(4\pi f t)\cos(2\pi f \tau_g) + \sin(4\pi f t)\sin(2\pi f \tau_g). \end{aligned} \tag{A.3}$$

The geometric delay τ_g changes slowly with Earth's rotation when tracking a source, see Fig. 2.2. The variation of $f\tau_g$ is many orders of magnitude smaller then the variations in ft. Hence, the rapidly varying terms in Eq. (A.3) is filtered out leaving us with the cross-correlation or fringe function:

$$r(\tau_g) = v_1 v_2 \cos(2\pi f \tau_g). \tag{A.4}$$

Appendix B

Extrasolar planets

Planet	D[pc]	M_J	d[AU]	T[days]	ω/ω_J	f_c[MHz]	$\log(I)$	$\log(P_{\rm rad})$
HD 41004 B b	43.0	18.40	0.018	1.33	0.31	1846.38	-3.50	16.81
GJ 436 b	10.2	0.07	0.028	2.63	0.16	0.08	-1.69	13.03
HD 189733 b	19.3	1.15	0.031	2.22	0.19	10.88	-2.75	14.64
HD 63454 b	35.8	0.38	0.036	2.82	0.15	1.35	-3.20	13.82
HD 73256 b	36.5	1.87	0.037	2.55	0.16	21.30	-3.48	14.75
55 Cnc e	13.4	0.05	0.038	2.81	0.15	0.04	-2.07	12.55
HD 46375 b	33.4	0.25	0.041	3.02	0.14	0.62	-3.16	13.46
Gl 581 b	6.3	0.06	0.041	5.37	0.08	0.03	-1.44	12.40
HD 179949 b	27.0	0.95	0.045	3.09	0.13	5.68	-3.24	14.16
Tau Boo b	15.0	3.90	0.046	3.31	0.13	55.77	-2.94	14.93
HD 75289 b	28.9	0.42	0.046	3.51	0.12	1.28	-3.18	13.63
HD 102195 b	29.0	0.49	0.049	4.11	0.10	1.41	-3.23	13.62
51 Peg b	14.7	0.47	0.052	4.23	0.10	1.28	-2.68	13.54
Ups And b	13.5	0.69	0.059	4.62	0.09	2.23	-2.74	13.65
HD 162020 b	31.3	13.75	0.072	8.43	0.05	179.07	-3.99	15.03
HD 217107 b	37.0	1.33	0.073	7.13	0.06	4.32	-3.82	13.73
HD 69830 b	12.6	0.03	0.079	8.67	0.05	0.01	-2.38	11.48
HD 130322 b	30.0	1.08	0.088	10.72	0.04	2.03	-3.70	13.34
HD 160691 d	15.3	0.04	0.090	9.55	0.04	0.01	-2.67	11.51
HD 108147 b	38.6	0.40	0.104	10.90	1	9.97	-4.18	13.76
Gl 86 b	11.0	4.01	0.110	15.77	1	464.56	-3.47	15.06
HD 4308 b	21.9	0.05	0.114	15.56	1	0.28	-3.44	12.46
55 Cnc b	13.4	0.78	0.115	14.67	1	30.60	-3.43	14.08
HD 99492 b	18.0	0.11	0.123	17.04	1	1.14	-3.45	12.90
HD 190360 c	15.9	0.06	0.128	17.10	1	0.39	-3.27	12.49
HD 195019 b	20.0	3.70	0.139	18.20	1	406.26	-4.14	14.85
HD 192263 b	19.9	0.72	0.150	24.35	1	26.55	-3.95	13.85
HD 69830 c	12.6	0.04	0.186	31.56	1	0.20	-3.27	12.00
Gliese 876 b	4.7	1.94	0.208	60.94	1	137.91	-3.07	14.19
rho CrB b	16.7	1.04	0.220	39.85	1	49.00	-4.12	13.80
HD 11964 b	34.0	0.11	0.229	37.62	1	1.16	-4.43	12.47
55 Cnc c	13.4	0.22	0.240	43.93	1	3.60	-3.76	12.83
HD 37605 b	42.9	2.30	0.250	55.00	1	183.94	-5.14	14.16
HD 117618 b	38.0	0.19	0.280	52.20	1	2.88	-4.75	12.65
HD 3651 b	11.0	0.20	0.284	62.26	1	3.14	-3.69	12.67
HD 168443 b	33.0	8.02	0.300	58.11	1	1474.87	-5.22	14.76
HD 114762 b	28.0	11.02	0.300	83.89	1	2504.77	-5.13	14.94
HD 219449 b	45.0	2.90	0.300	182.00	1	270.68	-5.34	14.17
HD 101930 b	30.5	0.30	0.302	70.46	1	6.17	-4.68	12.86
HD 178911 B b	46.7	6.29	0.320	71.49	1	984.27	-5.53	14.57
HD 16141 b	35.9	0.23	0.350	75.56	1	3.96	-4.88	12.60
HD 216770 b	38.0	0.65	0.460	118.45	1	22.39	-5.28	13.01
HD 93083 b	28.9	0.37	0.477	143.58	1	8.75	-4.98	12.66
70 Vir b	22.0	7.44	0.480	116.69	1	1301.43	-5.19	14.39
HD 52265 b	28.0	1.13	0.490	118.96	1	56.27	-5.13	13.29
GJ 3021 b	17.6	3.32	0.490	133.82	1	339.13	-4.89	13.91
HD 37124 b	33.0	0.61	0.530	154.46	1	20.14	-5.24	12.88

Planet	D[pc]	M_J	d[AU]	T[days]	ω/ω_J	f_c[MHz]	$\log(I)$	$\log(P_{\rm rad})$
HD 69830 d	12.6	0.06	0.630	197.00	1	0.40	-4.18	11.40
HD 82943 c	27.5	2.01	0.746	219.00	1	146.93	-5.49	13.33
HD 8574 b	44.2	2.23	0.760	228.80	1	174.71	-5.93	13.37
HD 134987 b	25.0	1.58	0.780	260.00	1	98.38	-5.41	13.16
HD 169830 b	36.3	2.88	0.810	225.62	1	267.58	-5.85	13.48
HD 40979 b	33.3	3.32	0.811	267.20	1	339.13	-5.79	13.56
HD 150706 b	27.2	1.00	0.820	264.00	1	45.90	-5.45	12.86
Ups And c	13.5	1.98	0.830	241.52	1	143.30	-4.95	13.24
HD 202206 b	46.3	17.40	0.830	255.87	1	5362.66	-6.34	14.50
HD 12661 b	37.2	2.30	0.830	263.60	1	183.94	-5.85	13.33
HD 89744 b	40.0	7.99	0.890	256.61	1	1465.69	-6.15	14.00
HR 810 b	15.5	1.94	0.910	311.29	1	138.51	-5.13	13.17
HD 160691 e	15.3	0.52	0.921	310.55	1	15.53	-4.94	12.40
HD 92788	32.8	3.86	0.970	377.70	1	435.96	-5.93	13.52
HD 142 b	20.6	1.00	0.980	337.11	1	45.90	-5.33	12.73
HD 28185 b	39.4	5.70	1.030	383.00	1	834.81	-6.18	13.71
HD 142415 b	34.2	1.62	1.050	386.30	1	102.56	-5.89	12.97
HD 128311 b	16.6	2.18	1.099	448.60	1	168.23	-5.34	13.10
HD 33564 b	21.0	9.10	1.100	388.00	1	1820.54	-5.75	13.93
HD 210277 b	22.0	1.23	1.100	442.10	1	64.81	-5.50	12.77
HD 196885 b	33.0	1.84	1.120	386.00	1	126.81	-5.92	12.99
HD 27442 b	18.1	1.28	1.180	423.84	1	69.26	-5.38	12.75
HD 82943 b	27.5	1.75	1.190	441.20	1	116.64	-5.80	12.92
HD 114783 b	22.0	0.99	1.200	501.00	1	45.14	-5.53	12.59
HD 20367 b	27.0	1.07	1.250	500.00	1	51.38	-5.75	12.60
HD 147513 b	12.9	1.00	1.260	540.40	1	45.90	-5.10	12.56
HIP 75458 b	31.5	8.82	1.275	511.10	1	1728.14	-6.20	13.81
HD 19994 b	22.4	2.00	1.300	454.00	1	145.72	-5.70	12.94
HD 222582 b	42.0	5.11	1.350	572.00	1	695.82	-6.41	13.45
HD 20782 b	36.0	1.80	1.360	585.86	1	122.25	-6.13	12.85
HD 65216 b	34.3	1.21	1.370	613.10	1	63.06	-6.04	12.61
HD 160691 b	15.3	1.67	1.500	654.50	1	107.89	-5.44	12.73
HD 141937 b	33.5	9.70	1.520	653.22	1	2024.96	-6.39	13.74
HD 114386 b	28.0	0.99	1.620	872.00	1	45.14	-5.95	12.38
HD 37124 d	33.0	0.60	1.640	843.60	1	19.59	-6.02	12.08
HD 23079 b	34.8	2.61	1.650	738.46	1	227.09	-6.29	12.93
HD 4208 b	33.9	0.80	1.670	812.20	1	31.64	-6.10	12.24
16 Cyg B b	21.4	1.68	1.680	799.50	1	108.97	-5.82	12.66
HD 62509 b	10.3	2.90	1.690	589.64	1	270.68	-5.27	12.97
HD 128311 c	16.6	3.21	1.760	919.00	1	320.61	-5.72	13.00
HD 81040 b	32.6	6.86	1.940	1001.70	1	1136.77	-6.49	13.37
HD 111323 b	29.0	6.80	1.970	1143.00	1	1120.24	-6.39	13.36
HD 213240 b	40.8	4.50	2.030	951.00	1	562.97	-6.65	13.10
Gamma Cephei b	11.8	1.60	2.044	902.90	1	100.46	-5.43	12.50
HD 114729 b	35.0	0.82	2.080	1131.48	1	32.97	-6.29	12.10
HD 10647 b	17.3	0.91	2.100	1040.00	1	39.22	-5.70	12.15
47 Uma b	13.3	2.60	2.110	1083.20	1	225.64	-5.62	12.75
HD 1644922	21.9	0.36	2.110	1155.00	1	8.36	-5.77	11.61
HD 10697 b	30.0	6.12	2.130	1077.91	1	939.83	-6.46	13.24
Gj 849 b	8.8	0.82	2.350	1890.00	1	32.97	-5.17	12.01

Planet	D[pc]	M_J	d[AU]	T[days]	ω/ω_J	f_c[MHz]	$\log(I)$	$\log(P_{\rm rad})$
HD 50554 b	31.0	4.90	2.380	1279.00	1	648.82	-6.54	13.04
Ups And d	13.5	3.95	2.510	1274.60	1	453.03	-5.82	12.87
HD 202206 c	46.3	2.44	2.550	1383.40	1	202.98	-6.83	12.59
HD 12661 c	37.2	1.57	2.560	1444.50	1	97.34	-6.58	12.33
HD 216437 b	26.5	2.10	2.700	1294.00	1	158.06	-6.36	12.46
HD 216435 b	33.3	1.49	2.700	1442.92	1	89.22	-6.51	12.26
14 Her b	18.1	4.64	2.770	1773.40	1	592.46	-6.17	12.90
HD 142022 A b	35.9	4.40	2.800	1923.00	1	542.27	-6.76	12.86
HD 11964 c	34.0	0.70	3.167	1940.00	1	25.33	-6.53	11.71
HD 37124 c	33.0	0.68	3.190	2295.00	1	24.31	-6.51	11.69
HD 39091 b	20.6	10.35	3.290	2063.82	1	2256.14	-6.51	13.24
HD 70642 b	29.0	2.00	3.300	2231.00	1	145.72	-6.57	12.29
Epsilon Eridani b	3.2	1.55	3.390	2502.00	1	95.28	-4.64	12.13
HD 33636 28.7	28.7	9.28	3.560	2447.29	1	1880.95	-6.84	13.12
HD 169830 c	36.3	4.04	3.600	2102.00	1	470.36	-6.93	12.64
HD 117207 b	33.0	2.06	3.780	2627.08	1	153.08	-6.78	12.21
HD 168443 c	33.0	18.10	3.910	1765.80	1	5727.02	-7.13	13.45
HD 190360 b	15.9	1.50	3.920	2891.00	1	90.42	-6.13	12.01
HD 89307 b	33.0	2.73	4.150	3090.00	1	244.76	-6.89	12.31
HD 160691 c	15.3	3.10	4.170	2986.00	1	302.51	-6.25	12.38
HD 217107 c	37.0	2.50	4.410	3352.00	1	211.36	-7.02	12.22
55 Cnc d	13.4	3.92	5.257	4517.40	1	447.31	-6.33	12.36
47 Uma c	13.3	1.34	7.730	2.59	1	74.75	-6.43	11.47
HD 106252 b	37.4	6.81	261.000	1500.00	1	1122.99	-10.01	9.96

Table B.1: All planets, within 40 pc from our solar system and a few more at distances longer then 40 pc but with very large masses, detected with the radial velocity method.

Bibliography

[1] G. B. Taylor, C. L. Carilli, and R. A. Perley, "*Synthesis Imaging in Radio Astronomy II*", San Francisco: Astronomical Society of the Pacific, cop. 1999.

[2] J. A. Zensus, P. J. Diamond, and P. J. Napier, "*Very long baseline interferometry and the VLBA*, San Francisco: Astronomic Society of the Pacific, 1995.

[3] Wiley J. Larson and James R. Wertz, "*Space Mission Analysis And Design*", El Segundo, CA.: Microcosm; Dordrecht: Kluwer, cop. 1999.

[4] A. Richard, Thompson, "*Interferometry and synthesis in radio astronomy*", New York: Wiley, cop. 2001.

[5] Bernard F. Bruke, "*An introduction to radio astronomy*", New York: Cambridge Univ. Press, 1997.

[6] Monson H. Hayes, "*Statistical digital signal processing and modeling*", New York: Wiley, cop. 1996.

[7] Kepler Mission, http://kepler.nasa.gov

[8] SIM PlanetQuest, http://planetquest.jpl.nasa.gov/SIM/new_worlds.cfm

[9] Terrestrial Planet Finder, http://planetquest.jpl.nasa.gov/TPF/tpf_book/index.cfm

[10] Karl Jansky and the Discovery of Cosmic Radio Waves, National Radio Astronomy Observatory, http://www.nrao.edu/whatisra/hist_jansky.shtml

[11] K. I. Kellerman and J. M. Moran "*The Development of High-Resolution Imaging in Radio Astronomy*", Annual Review of Astronomy and Astrophysics, Vol. 39:457-509

[12] Jaap D. Bregman, "*Design Concepts for a Sky Noise Limitied Low Frequency Array*", ASTRON, 2000

[13] Joint Statement, European Lunar Observatories Science Workshop, http://www.astron.nl/moon/pdf/Joint_Statement.pdf

[14] T. S. Bastian, G. A. Dulk, and Y. Leblanc, "*A Seacrh for Radio Emission from Extrasolar Planets*", The Astrophysical Journal, Vol. 545:1058-1063

[15] 181 Things To Do On The Moon, http://science.nasa.gov/headlines/y2007/02feb_181.htm?list123680

[16] T. Joseph, W. Lazio, and W. M. Farrell, "*The Radiometric Bode's Law and Extrasolar Planets*", The Astrophysical Journal, Vol. 612:511-518

[17] Jaap D. Bregman, "*Concept design for a low frequency array*", Proceedings of SPIE, Vol. 4015:19-32

[18] Eugene Hecht, "*Optics*, Addison-Wesley, cop. 2002.

[19] W. L. Imhof, S. M. Pentrinec, R. R. Anderson, M. Walt, J. Mobilia, and H. Matsumoto, "*Correlations between low-frequency and high-frequency auroral kilometric radiation plasma wave intensity bursts and X-rays in the auroral zone*", Journal of Geophysical Research, Vol. 109:A09204